

Visualization of the Domain Structure of an L-type Ca^{2+} Channel Using Electron Cryo-microscopy

M. Wolf^{1,2}, A. Eberhart², H. Glossmann², J. Striessnig² and N. Grigorieff^{1*}

¹Howard Hughes Medical Institute, Brandeis University Rosenstiel Center (MS029) 415 South Street, Waltham MA 02454-9110, USA

²Institute for Biochemical Pharmacology, Peter-Mayr Str. 1, A-6020 Innsbruck, Austria

The three-dimensional structure of the skeletal muscle voltage-gated L-type calcium channel ($\text{Ca}_v1.1$; dihydropyridine receptor, DHPR) was determined using electron cryo-microscopy and single-particle averaging. The structure shows a single channel complex with an approximate total molecular mass of 550 kDa, corresponding to the five known subunits of the DHPR, and bound detergent and lipid. Features visible in our structure together with antibody labeling of the β and α_2 subunits allowed us to assign locations for four of the five subunits within the structure. The most striking feature of the structure is the extra-cellular α_2 subunit that protrudes from the membrane domain in close proximity to the α_1 subunit. The cytosolic β subunit is located close to the membrane and adjacent to subunits α_1 , γ and δ . Our structure correlates well with the functional and biochemical data available for this channel and suggests a three-dimensional model for the excitation–contraction coupling complex consisting of DHPR tetrads and the calcium release channel.

© 2003 Elsevier Ltd. All rights reserved.

Keywords: voltage-gated calcium channel subunits; immuno labeling; single-particle image processing; tetrad; excitation–contraction coupling complex

*Corresponding author

Introduction

Voltage-gated L-type calcium channels play an essential physiological role in excitation–contraction (EC) coupling, calcium homeostasis, gene regulation and hormone secretion. Different isoforms of these ion channels were found in skeletal ($\text{Ca}_v1.1$), smooth ($\text{Ca}_v1.2$) and cardiac muscle ($\text{Ca}_v1.2$, $\text{Ca}_v1.3$). They are characterized by intermediate or high voltage of activation, large single channel conductance, slow voltage-dependent inactivation, regulation by cAMP-dependent

protein phosphorylation pathways and specific inhibition by calcium-antagonist drugs including dihydropyridines (DHPs), phenylalkylamines and benzothiazepines.¹ They share a common architecture consisting of five subunits (α_1 , α_2 , β , γ , and δ). The α_2 and δ subunits originate from the same gene, but are post-translationally cleaved and disulfide-linked, resulting in the composite subunit $\alpha_2\delta$.^{2,3} The function of skeletal muscle L-type calcium channels ($\text{Ca}_v1.1$; dihydropyridine receptor; DHPR) lies mainly in EC coupling. Mutations in this channel lead to inheritable human diseases, such as malignant hyperthermia and hypokalemic periodic paralysis.⁴ The L-type calcium channels take part in the signal transduction mechanism that relays an excitatory depolarization in the tubular membrane to the calcium release channel in the sarcoplasmic membrane. Rapid depolarization-induced conformational changes of DHPR stimulate calcium efflux from the sarcoplasmic reticulum (SR) through the calcium release channel (CRC, or ryanodine receptor, RyR), which subsequently trigger the contractile apparatus until the calcium concentration is reduced again due to re-uptake into the SR by the Ca^{2+} -ATPase (Serca1). Small calcium currents through the DHPR are

Present addresses: J. Striessnig, Department of Pharmacology and Toxicology, Institute of Pharmacy, Peter-Mayrstr. 1/I, A-6020 Innsbruck, Austria; M. Wolf, Howard Hughes Medical Institute, Brandeis University, Rosenstiel Center (MS029), 415 South Street, Waltham, MA 02454-9110, USA.

Abbreviations used: DHPR, dihydropyridine receptor; EC, excitation–contraction; SR, sarcoplasmic reticulum; CRC, calcium release channel; RyR, ryanodine receptor; EM, electron microscopy; CTF, contrast transfer function; FSC, Fourier shell correlation; AID, alpha interaction domain; DDM, *n*-dodecyl- β -D-maltoside.

E-mail address of the corresponding author: niko@brandeis.edu

activated slowly and are not sufficient to trigger muscle contraction in skeletal muscle. It is widely accepted that physical coupling accounts for the close functional coupling between the DHPR and the RyR in skeletal muscle.⁵ So far the exact mechanism of EC coupling is not fully understood and no high-resolution structural information on the DHPR or RyR is available.

Previous studies of the structure of the DHPR showed an asymmetrical particle^{6,7} or a circular structure that was interpreted as a channel dimer.⁸ None of these structures show sufficient detail to reveal the location of individual subunits or domains of the channel.

Here, we present the structure of the L-type Ca channel from skeletal muscle at 23 Å resolution, which allowed us to identify the locations of four of the five subunits of the channel. The proposed arrangement of the subunits provides a structural basis for the functional and biochemical data available for this channel and suggests a 3D model of the major part of the EC coupling complex formed by the two ion channels.

Results

Characterization of the purified channel

We performed experiments to assess the integrity and homogeneity of the purified channel complex.

Subunit composition

Purification was carried out after solubilization in digitonin according to published procedures,^{9,10} which have been shown to result in functionally active channels after reconstitution in lipid bilayers.⁹ Digitonin was chosen as a detergent because significant loss of $\alpha_2\delta$ and β subunits could be detected in other detergents, including 3-[(3-cholamidopropyl)-dimethylammonio]-1-propanesulphonate (Chaps) and *n*-dodecyl- β -D-malto-side (DDM) (data not shown). Silver-staining of purified preparations separated by SDS-PAGE (7% or 10% (w/v) separation gels; **Figure 1A**) showed five major bands migrating with apparent molecular masses ($\alpha_1 = 176(\pm 13)$ kDa, $\alpha_2 = 147(\pm 9)$ kDa, $\beta = 56(\pm 2)$ kDa, $\gamma = 34(\pm 1)$ kDa, $\delta_1 = 28(\pm 0.5)$ kDa, $\delta_2 = 24(\pm 0.5)$ kDa; $n = 2$) corresponding to previously observed apparent molecular masses of the DHPR subunits.³ These bands comprised $94(\pm 4)\%$ ($n = 2$) of the total staining intensity, indicating high purity of the preparation. The α_1 subunit has been reported to migrate abnormally on SDS-PAGE and a molecular mass of 193 kDa was determined by Ferguson analysis.¹¹ α_2 and δ subunits are linked by a disulfide bridge and, accordingly, run as a single band under non-reducing conditions ($168(\pm 10)$ kDa; **Figure 1B**). The identity of the bands, corresponding to the α_1 , α_2 and β subunits, were further confirmed by Western blot using monoclonal

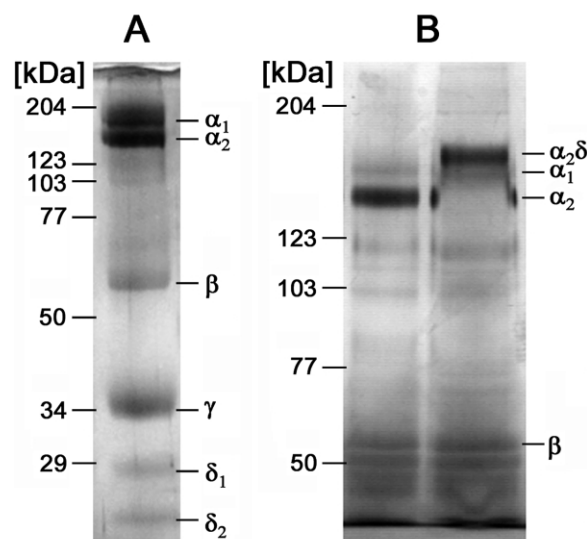


Figure 1. A, Silver-stained SDS-PAGE (10% separation gel) analysis of purified DHPR under reducing conditions. The molecular masses of the subunits as calculated from the migration of the indicated molecular mass standards were 176 kDa (α_1), 147 kDa (α_2), 56 kDa (β), 34 kDa (γ), 28 kDa (δ_1) and 24 kDa (δ_2). B, SDS-PAGE analysis (7% separation gel) under reducing (left lane) or non-reducing conditions (see Materials and Methods). Under non-reducing conditions the $\alpha_2\delta$ subunit migrated at higher molecular mass than α_1 , illustrating the integrity of the disulfide-linked $\alpha_2\delta$ subunit.

antibodies (see Materials and Methods; data not shown). The two bands at 28 kDa and 24 kDa most likely represent two variants of the δ peptide, δ_1 and δ_2 , that show different degrees of glycosylation.³

Channel homogeneity

Velocity sedimentation analysis of the purified DHPR in an analytical ultracentrifuge (**Figure 2**) revealed a predominant molecular species with a sedimentation coefficient of 8.8 S when solubilized with digitonin. These results suggest that our preparation contains single channel complexes, consistent with previously published results using a similar purification protocol.⁷ In contrast, the Chaps and DDM-solubilized channel yielded multiple peaks at lower *s* values and increasing amounts of protein at values greater than 8.8 S. This suggests that significant complex dissociation and aggregation happens in these detergents. The monodispersity of our preparation was confirmed by electron microscopy (EM) of negatively stained samples (**Figure 3**), showing isolated particles of about 170 Å diameter. Gel-filtration chromatography yielded a homogeneous peak corresponding to a molecular mass of about 800 kDa for the DHPR–digitonin complex (data not shown). This value is consistent with a monodisperse channel complex and suggests that the

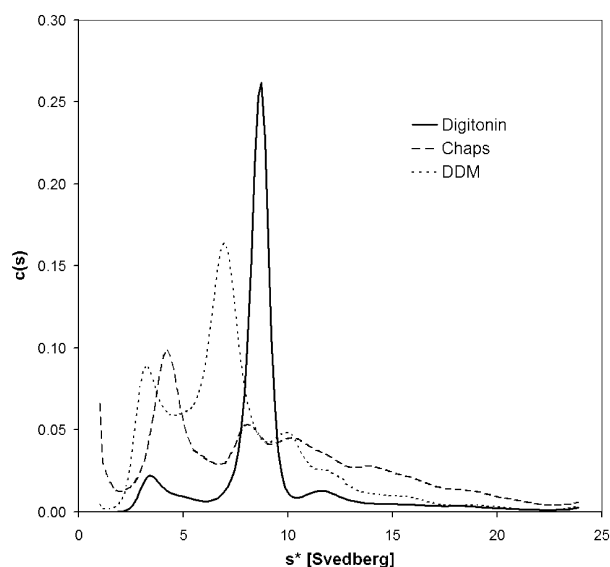


Figure 2. Analytical ultracentrifugation of purified DHPR preparation performed in standard buffer (see Materials and Methods). Sedimentation velocity analysis was performed using the program SEDFIT⁴⁶ and sedimentation coefficients were plotted *versus* frequency of occurrence $c^*(s)$. The s -values were not corrected for temperature or buffer viscosity. The digitonin-solubilized material sediments as one predominant peak at 8.8 S, indicating a homogeneous population of particles with a uniform size distribution. The use of Chaps and n -dodecyl- β -D-maltoside (DDM) both led to significant dissociation and aggregation of channel complexes.

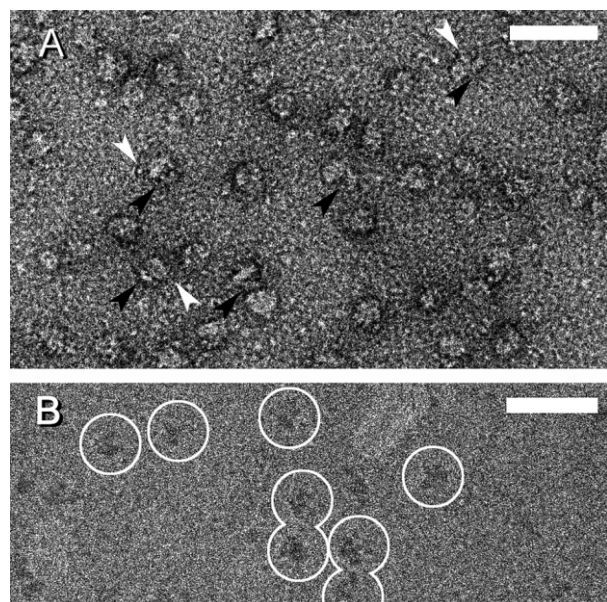


Figure 3. A, Section of a micrograph (recorded at 60,000 \times magnification) showing negatively stained monodisperse single particles. A leg-shaped protrusion is clearly visible in individual particles (black arrows). Another smaller protrusion is visible on the opposite side of the channel particle (white arrows). B, Section of a micrograph (recorded at 62,000 \times magnification) showing single channels (circled) in ice at 3 μ m under-focus. The scale bars represent 50 nm.

isolated complex contains several hundred kDa of associated detergent (see Discussion).

Electron microscopy and image processing

3D structure of the channel

We determined the 3D structure of the channel by EM and single-particle averaging using both negatively stained samples at room temperature, and frozen-hydrated samples at liquid nitrogen temperature (cryo-EM). Negatively stained samples display enhanced contrast, simplifying the initial determination of a 3D structure. However, this technique is known to produce artifacts, such as flattening of the sample and partial staining. These problems are absent from frozen-hydrated samples, but the alignment of the channel particles becomes more difficult because of much reduced image contrast. We used the 3D structure obtained from negatively stained samples to verify the overall shape of a second structure determined independently from frozen-hydrated samples, thereby ensuring a successful alignment of the low-contrast images.

Figure 4 shows the processing of images from negatively stained samples. The principle features of the 3D structure consist of a large globular domain and a long “leg-shaped” protrusion. These features are also clearly visible in some of the raw images (Figure 3) and class averages. The class averages from 7572 images of channels agree well with re-projections of the final 3D structure, demonstrating that the structure is consistent with the class averages.

A total of 15,229 images of frozen-hydrated channel particles were collected from micrographs recorded on a field emission electron microscope

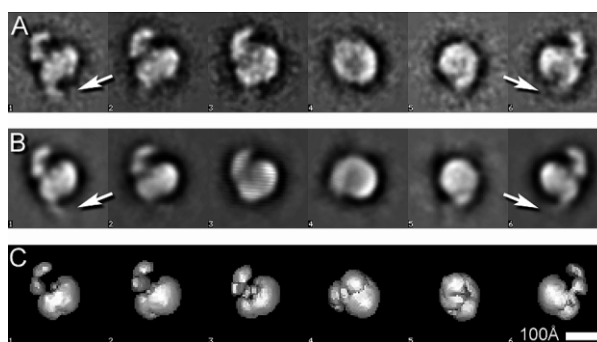


Figure 4. Six representative class averages of negatively stained channels (A), each containing on average 40 members with identical views. The class averages were processed using the IMAGIC software¹² and agree well with their re-projections (B) of the 3D structure (volume rendering, C), demonstrating that the structure is consistent with the class averages. The principal features of the 3D structure consist of a large globular domain and a leg-shaped protrusion that is also clearly visible in some of the raw images (Figure 3) and class averages. The white arrows point to the location of a smaller protrusion that appears with a lower density in the averaged images. This feature is not well resolved.

at 200 kV. The initial 3D structure obtained using the IMAGIC image processing package¹² was refined and corrected for the contrast transfer function (CTF) using the computer program FREALIGN.¹³ The initial structure before refinement is shown in Figure 5C and displays a hole in the center of the large globular domain. This hole disappeared after correcting the data for the CTF. The final 3D structure is shown in Figure 6, using two different contour levels to illustrate the density distribution inside the globular domain. The larger volume in Figure 6 corresponds to a total molecular mass of 550 kDa, assuming an average protein density of 1.22 g/cm³ or 0.735 Da/Å³.¹⁴ The total molecular mass of 550 kDa assumes the presence of all five subunits of the channel, as well as detergent and residual lipid (see Discussion). At the higher contour level, the globular density is divided by a gap into a larger and smaller density, indicating possible boundaries of channel subunits. The angular distribution of particle orientations (Figure 7) shows that most orientations are represented in our data set, thereby minimizing any artifacts due to insufficient sampling. The Fourier shell correlation (FSC) plot (Figure 8) indicates a resolution of 23 Å at a value of 0.5.

The globular domain has the shape of an ellipsoid with a length of 165 Å, a width of 145 Å and a height of about 80 Å. The leg-shaped protrusion has a length of about 95 Å and is attached off-center on one of the flat sides of the globular domain. Based on its volume, the protrusion has a molecular mass of 100 kDa. When dividing the globular domain along the gap visible at a higher density contour level (Figure 6), the molecular masses of the smaller and larger sub-volumes are 120 kDa and 330 kDa, respectively.

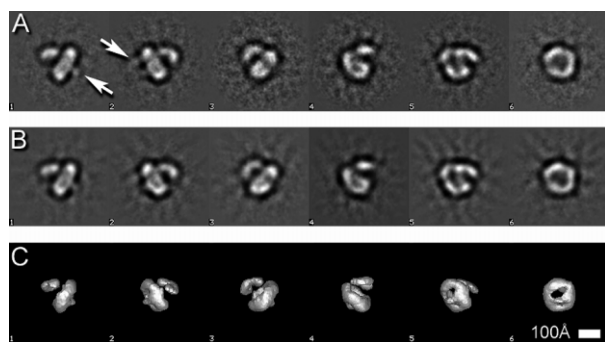


Figure 5. Six representative class averages of channels embedded in ice (A), each containing on average 180 members with identical views. The class averages were processed using the IMAGIC software¹² and agree well with their re-projections (B) of the 3D structure (C). The cryo reconstruction agrees in its overall shape with the reconstruction from negatively stained images. The most obvious difference is the hollow appearance of the cryo 3D structure. This hole disappeared after correcting the data for the contrast transfer function of the electron microscope.

Immunolabeling

In order to locate channel subunits within our 3D structure, we labeled the DHPR with monoclonal antibodies directed against the extracellular α_2 subunit and the intracellular β subunit. Unbound antibodies were removed by size-exclusion chromatography. Figure 9 shows images of negatively stained channels labeled with anti- α_2 and anti- β antibodies. To clearly identify the antibody-binding site, an average of each of the images shown in Figure 9 was calculated (framed in black). Compared with the unlabeled channel (see Figure 4), additional density appears on the side of the leg-shaped protrusion in the presence of anti- α_2 antibody. The anti- β antibody generates extra density close to the globular domain on the opposite side of the large protrusion.

Discussion

We present here the 3D structure of the skeletal muscle L-type calcium channel determined at 23 Å resolution using cryo-EM and single-particle averaging. Channels were purified and characterized following a standard protocol, which has been shown to result in functionally active channels, yielding homogeneous and monodisperse protein. Our structure has higher resolution compared with previous studies and we were able to identify the locations of the α_2 and β subunits by antibody labeling. These results and other biochemical data allow us to map the approximate locations of four of the five subunits of the DHPR complex. The domain structure of the DHPR suggests a model for the arrangement of the DHPR and RyR in the EC coupling complex.

Interpretation of the density map

The resolution of our structure does not allow direct identification of the domain structure of the DHPR from the density map. However, the surface representation of the electron density map shows a globular domain with a leg-shaped protrusion, when contoured at a density level that results in an overall molecular mass of 550 kDa. The total mass of 550 kDa exceeds the combined molecular mass of all the channel subunits by about 100 kDa. However, if the structure is contoured at a density level including only 450 kDa, the leg-shaped protrusion clearly visible in the class averages (Figure 5A) disappears. As discussed below, the extra density is likely to be due to detergent and residual lipid bound to the channel.

Using antibody labeling, the leg-shaped protrusion was identified as the α_2 subunit, which is located on the extracellular or t-tubular side of the channel.¹⁵ We located the binding site of the anti- β antibody within the smaller of the two sub-volumes of the globular domain. The β subunit is known to be located on the intracellular side of

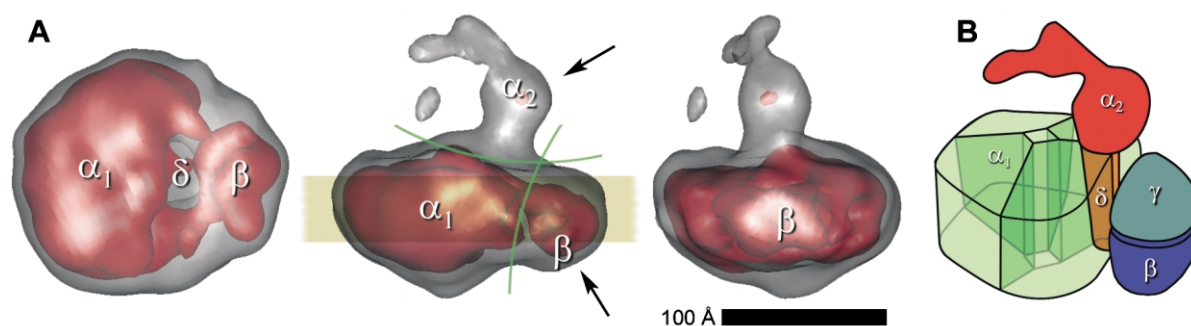


Figure 6. A, Three orthogonal views of the refined 3D structure of the dihydropyridine receptor, filtered at 23 Å resolution. The reconstruction was corrected for the contrast transfer function of the electron microscope. The volume in gray encloses approximately 550 kDa. When contoured at a higher density level (red volume), the globular density is separated by a gap into a larger and smaller density, indicating possible boundaries of channel subunits. Labels indicate the putative locations of individual subunits. Left: view facing the cytosolic side. Middle: view along the membrane plane (depicted by a yellow bar) with the extracellular α_2 subunit facing upwards. The green arcs indicate how the structure was divided to estimate the molecular masses of individual subunits (see Discussion). The two arrows point to approximate binding locations of the respective monoclonal antibodies. The size of the β subunit is most likely underestimated in this rendering (see Discussion). Right: view along the membrane plane after rotating the structure by 90° from its orientation shown in the middle panel. The surface views were generated with the molecular viewer CHIMERA (<http://www.cgl.ucsf.edu/chimera>).⁴⁸ B, Cartoon of the L-type calcium channel, summarizing our results together with previously published data on subunit interactions. It assumes pseudo-4-fold symmetry of the α_1 -subunit. The view shows the extracellular side with the α_2 subunit. The α_1 , γ and δ subunits are embedded into the lipid membrane (not shown), which separates the extracellular α_2 subunit from the cytosol. α_2 is anchored via the disulfide-linked δ subunit within the α_1 subunit. The proposed model allows for a tight interaction between α_1 and δ as well as α_1 and γ .

the channel facing the RyR in intact EC coupling complexes.¹⁶ Thus, the arrangement of α_2 and β subunits on opposite sides of the globular domain implies that the globular domain must contain the membrane-embedded subunits of the channel. It also indicates the approximate orientation of the channel in the cell membrane, as shown in

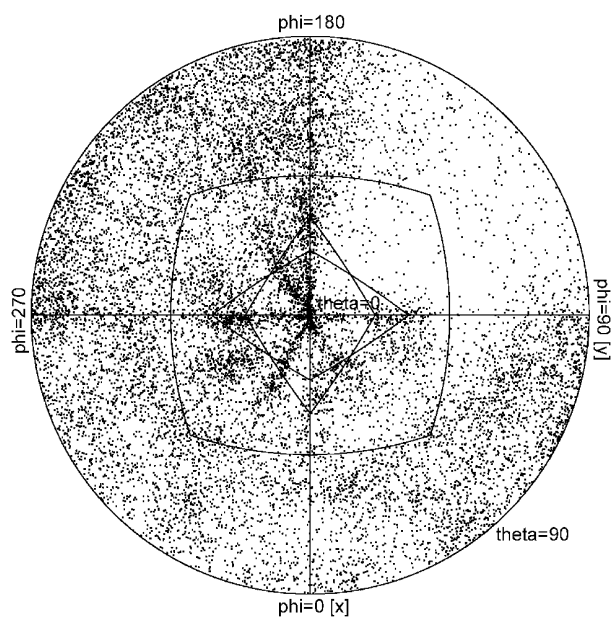


Figure 7. The angular distribution of particle orientations shows that most orientations are represented in the data set, thereby minimizing any artifacts due to insufficient sampling.

Figure 6. Our class-averages show a weak density feature at the location of the β subunit (arrow in Figures 4B and 5A), that is not clearly resolved in the 3D reconstruction. The weak appearance of density corresponding to the β subunit could indicate some flexibility in this part of the structure.

The pore-forming α_1 subunit consists of four conserved domains with six transmembrane segments each. These domains are thought to be arranged in a pseudo-tetrameric structure.¹⁷ However, we cannot clearly identify 4-fold features in our structure. The globular domain breaks up into two sub-volumes when the channel structure is contoured at a higher density level, indicating a possible domain boundary. Only the larger of the

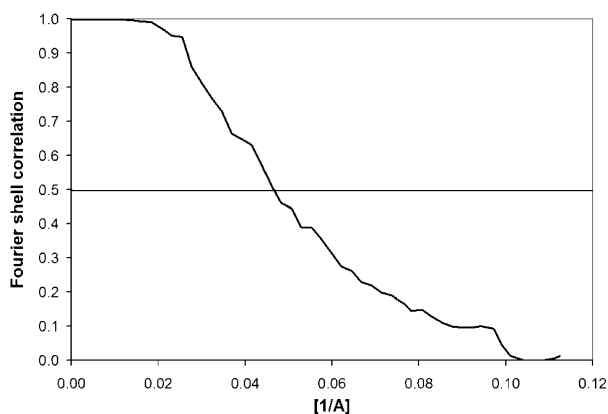


Figure 8. The Fourier shell correlation plot indicates a resolution of 23 Å at a correlation of 0.5.

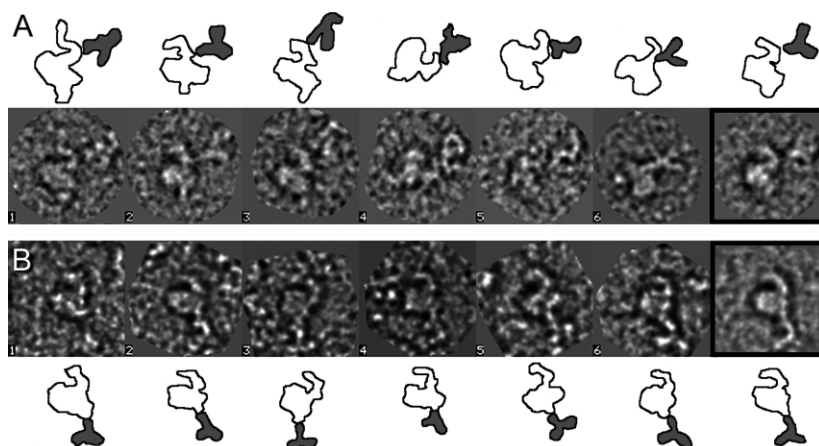


Figure 9. Images of negatively stained DHPR labeled with monoclonal antibodies targeting the α_2 subunit (A) or the β subunit (B). The particles show similar side views of the channel. Since the conformation of the bound antibodies varies from image to image, an average of the images in each was calculated (framed in black) to highlight the antibody-binding sites that remain constant in each image. Compared with the unlabeled channel (see Figure 4), additional density appears on the side of the leg-shaped protrusion in the presence of anti- α_2 antibody. The anti- β antibody produces extra density close to the globular domain on the opposite side of the large protrusion.

two sub-volumes provides sufficient room to accommodate the 190 kDa α_1 subunit (Table 1 and Figure 6). The α_2 and δ subunits are linked by a disulfide bridge and the small δ subunit consists of a single membrane-spanning helix.^{3,15} Our reconstruction shows that the α_2 subunit protrudes from one side of the larger sub-volume of the globular domain, close to the density gap within that domain. This suggests that the δ subunit is adjacent to or partially embedded within the α_1 subunit. These conclusions are consistent with *in vitro* protein association assays described by Gurnett *et al.*¹⁸ that show that α_2 does not assemble with the cardiac α_{1c} subunit in the absence of the δ subunit. The association assays suggest that the $\alpha_2\delta$ subunit likely interacts with more than one extra-cellular loop of the α_1 subunit. Moreover, in the presence of reducing agents, α_2 can be extracted at alkaline pH, while δ remains membrane-associated.³ Taken together, these obser-

vations suggest a tight interaction of δ with the α_1 subunit, in agreement with our structure.

The membrane-embedded γ subunit¹⁹ can either be located in the small or in the large sub-volume of the globular domain. The γ_1 subunit has been shown to associate with the α_1 subunit in recent co-sedimentation experiments.²⁰ Channels lacking the γ subunit are functional with altered channel inactivation properties,²¹ and α_1 , β and $\alpha_2\delta$ are still associated in γ_1 null mice.²⁰ This suggests a more peripheral location of the γ subunit, contacting the α_1 subunit but none of the other subunits. According to our structure, however, it appears more likely that the γ subunit occupies part of the small sub-volume, since the known molecular mass of the β subunit accounts for only half of the calculated mass associated with the small sub-volume (Table 1). If the γ subunit is located in the small sub-volume, it would be in close proximity to the α_1 , β and δ subunits. This close arrangement of subunits does not contradict the results cited above because sufficient interaction between the subunits remains to form a complex even in the absence of the γ subunit. For example, the β subunit interacts directly with the α_1 subunit I–II loop and the alpha interaction domain (AID).^{22–24} Figure 6B summarizes the domain structure of the DHPR displaying the features described above.

There is a discrepancy between the molecular masses associated with the measured volumes of the different parts of the channel, and the known molecular masses of the subunits assigned to these volumes. The leg-shaped protrusion identified as the α_2 subunit appears to be too small to accommodate the entire α_2 subunit including glycosylation. The smaller observed volume could be the result of flexibility of this subunit, the covalently attached polysaccharides, or both. This flexibility would lead to a loss of density when averaging over different conformations of the α_2 subunit. The volume of the globular domain is

Table 1. Molecular mass estimates

Density	Molecular mass according to volume (kDa)	Molecular mass, as published (kDa)
A. Leg-shaped protrusion		
α_2 -volume	100	150
B. Globular domain		
β - γ -volume	120	84
α_1 - δ -volume	330	218
Total	550	452

If the volume of the 3D reconstruction is divided along the green arcs, as shown in Figure 6, the molecular masses of most subunits can be estimated assuming an average protein density of 1.22 g/cm³ or 0.735 Da/Å³.¹⁴ The total molecular mass of 550 kDa assumes the presence of all five subunits of the channel, as well as detergent and residual lipid (see Discussion). The known molecular masses of all five subunits total 452 kDa and have been published elsewhere (α_1 = 193 kDa;¹¹ α_2 = 150 kDa, β = 52 kDa, γ = 32 kDa, δ = 25 kDa³).

equivalent to approximately 450 kDa of protein, exceeding the combined molecular mass of the α_1 , β , γ and δ subunits by about 150 kDa (Table 1). The excess molecular mass could, at least in part, be attributed to detergent bound to the channel. It was found that Shaker potassium channels solubilized in Chaps contained about 60 kDa of detergent per channel.²⁵ Digitonin has been reported to form micelles with an average molecular mass of at least 75 kDa,²⁶ which is about ten times larger than the molecular mass of Chaps micelles (6 kDa \dagger). Furthermore, digitonin is not as efficient as Chaps in solubilizing lipid,²⁷ and some residual lipid still bound to the DHPR may add to the mass of the globular domain. Therefore, the observed 150 kDa of additional mass in the globular domain can be explained with detergent and residual lipid bound to the membrane domain of the channel. We estimate the total molecular mass of the detergent-protein complex to be 600 kDa, which exceeds the mass of the contoured volume given in Figure 6 by 50 kDa due to the loss of density in flexible parts of the structure.

It has been suggested that the DHPR exists as a channel dimer.⁸ We obtained an approximate total molecular mass of 800 kDa by gel-filtration chromatography for the channel-detergent complex using molecular mass standards (data not shown), which closely matches a value of 740 kDa determined previously.²⁸ Based on the channel subunits alone, a channel dimer would have a total molecular mass of 900 kDa, and the presence of detergent would further increase this mass by several hundred kDa. We therefore believe the observed higher molecular mass of 800 kDa to be a consequence of the extended structure of the α_2 subunit that produces an overall shape of the channel much different from the globular standards used to calibrate the gel-filtration column. This conclusion is further backed up by previous results from ultracentrifugation that determined a significant deviation from an ideal spherical shape for the detergent-solubilized DHPR.²⁸ The presence of monodisperse channel complexes rather than channel dimers is also consistent with results published elsewhere⁷ that are based on a similar preparation protocol.

Functional implications and tetrad arrangement

In native skeletal muscle in the triad junction, DHPRs are arranged in groups of four. The arrangement of those tetrads in the t-tubular membrane corresponds to the arrangement of RyRs in the adjacent sarcoplasmic membrane.²⁹ The spacing between DHPRs (18.4(\pm 0.4) nm) as well as the inter-tetrad spacing that coincides with the inter-RyR spacing, has been determined accurately from images of tetrad arrays.³⁰ Based on the DHPR domain structure and the 3D structure of

RyR1,³¹ we propose a model for the functional interaction between the two ion channels in EC coupling (Figure 10A and B). In this model, the location of the α_1 subunit is indicated by a red square with dimensions close to the pore-forming α subunit of the Shaker potassium channel²⁵ and the recently solved crystal structure of a bacterial voltage-dependent K⁺ channel.³² In Figure 10A, domains I and II of the α_1 subunit have been placed close to β , according to known interactions between β and the long intracellular loop connecting domains I and II.^{23,33} The clockwise arrangement of the α_1 domains will be addressed below.

The orientation of DHPR relative to RyR1 is determined by a number of specific interactions between the two complexes. The carboxy terminus of the β_{1a} subunit is involved in EC coupling of skeletal muscle³⁴ and, therefore, must be close to RyR. Indeed, peptide fragments from three independent sites within RyR1 sequence 2169–3661 were found to interact with the DHPR β subunit,³⁵ with the strongest interaction involving fragment 3200–3600 (R. Coronado, personal communication). The binding site of apo-calmodulin has been located on the surface of RyR1 by EM³⁶ and corresponds to residues 3614–3643, which overlap with the sequence identified for the RyR1–DHPR- β interaction. Therefore, we oriented the DHPR with its β subunit pointing towards the apoCaM-binding site (Figure 10B).

Specific interactions between the DHPR II–III loop and RyR limit the possible tetrad arrangement further. The peptide C region (s53; residues 724–760) of the DHPR II–III loop participates in functional interaction with the RyR.³⁷ This sequence binds to the R16 region of RyR1 (residues 1837–2168) in yeast two-hybrid assays.³⁸ Recently, the divergent region 3 (DR3; residues 1872–1923 of RyR1) has been located (Figure 10A and B; region 9, yellow) by EM.³⁹ Since DR3 is part of R16, it is likely that the location of DR3 on the RyR is in close proximity of the DHPR II–III loop. To satisfy the distance constraint of approximately 18 nm³⁰ between DHPRs within a tetrad while bringing their II–III domains close to the DR3 regions of RyR and avoiding density overlap with the protruding region 6 of the RyR, the long axis of the globular domain of each DHPR has to be approximately parallel with the side of the roughly square RyR (see Figure 10A).

Finally, recent fluorescence resonance energy transfer (FRET) experiments⁴⁰ suggest an arrangement that minimizes the distance between N and C termini of neighboring DHPRs within a tetrad. This suggests that the C and N termini are on the inside of the tetrad, leading to a clockwise arrangement of the α_1 domains I–IV when viewed from the extra-cellular side. A clockwise arrangement of the α_1 domains would also be consistent with the only possible arrangement found by homology modeling.^{17,41}

Two motifs have been suggested for the formation of RyR arrays.⁴² More recently, one of them

\dagger Calbiochem Product Data Sheet 220201.

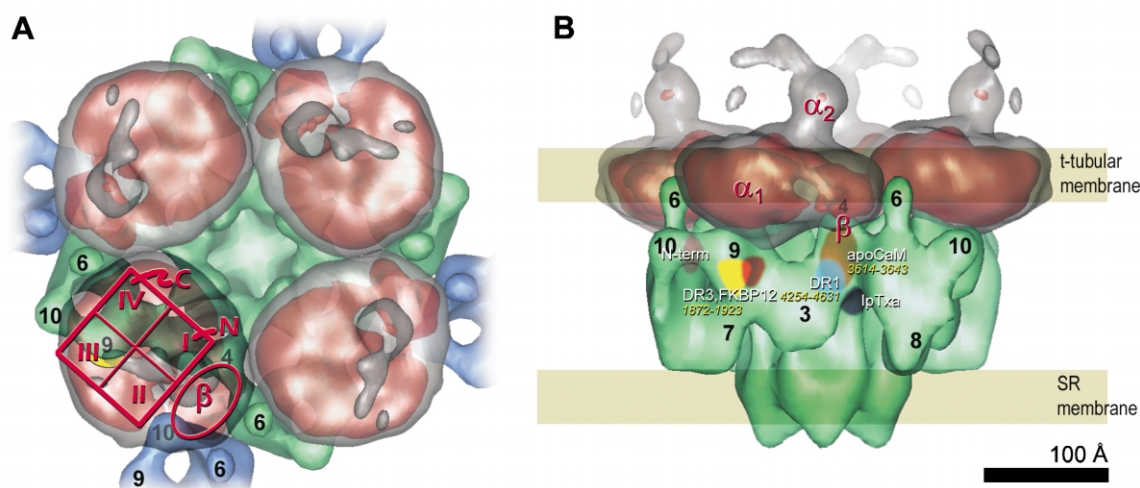


Figure 10. Model of DHPR–RyR complex. EC coupling in skeletal muscle is assumed to consist of a complex between the calcium release channel (RyR, green) and the voltage sensing L-type calcium channel (DHPR, grey and red). DHPRs are arranged in assemblies of four, called tetrads, on every other RyR. Views from the t-tubular side (A) and parallel (B) with the membranes. The red square in A indicates the putative α_1 domain structure. Divergent region 3 (DR3) of the RyR (yellow in A and B) can interact with fragments of the DHPR II–III loop.³⁸ Fragments overlapping with the apo-calmodulin-binding site (orange in B) were shown to bind to the DHPR β subunit.³⁵ The N terminus and parts of the C terminus are shown to point into the center of the tetrad (see Discussion). Inter-DHPR spacing is 18 nm. The height of the junctional gap as shown corresponds to 13.3 nm, consistent with the results of Takekura *et al.*⁴⁹ The inter-RyR spacing between tetrad-occupied RyRs is 42.9 nm, if RyRs are arranged as indicated by a neighboring RyR (blue structure). The black numbers designate RyR regions as used by Wagenknecht *et al.*⁴² The yellow numbers indicate RyR amino acid residues in the identified regions or binding sites (white text). Indicated locations: N terminus,^{50,51} DR3,³⁹ FKBP12,⁴² DR1,⁵² apoCaM,³⁶ IpTxa.³¹ The scale bar represents 100 Å.

was observed by electron tomography of isolated triad junctions,⁴³ and this is the motif indicated in our model shown in Figure 10A. The blue structures in Figure 10A indicate the corners of neighboring RyRs, in this motif.⁴² The array is also consistent with recently published two-dimensional crystals of RyRs.⁴⁴ With such an arrangement, the inter-tetrad spacing is 42.9 nm, in agreement with the spacing obtained from images of tetrad patterns in BC₃H1 cells ($41.9(\pm 1.6)$ nm),³⁰ as well as the inter-RyR spacing of 30.6 nm ($31.0(\pm 3.5)$ nm).³⁰ The orientation of the tetrads with respect to the two-dimensional lattice of RyRs corresponds to images from freeze-fractured, rotary-shadowed tetrad arrays, if we assume that the shadowing visualizes mainly the α_2 subunit that forms the highest elevation of the structure.

Comparison with previously determined structures

The structure of the DHPR has been determined in three previous publications,^{6–8} also using detergent-solubilized channel protein and EM of single molecules. The structures determined by Murata *et al.* and Serysheva *et al.* agree roughly in their dimensions with the structure we present here. Murata *et al.* based their model on a tentative assignment of views visible in the raw data and class averages. It features a channel pore of 200 Å

in length and was derived from labeling experiments of a single site using only anti- β antibody, which leaves an ambiguity in the orientation of the channel. Furthermore, the use of Chaps to solubilize the channel may have led to some aggregation, as suggested by the analytical ultracentrifugation experiments shown in Figure 2B.

The structure described by Serysheva *et al.* was determined at a lower resolution and does not show any of the details we report here. However, the location of the α_2 subunit is consistent with our model and the shape of the two structures agree when compared at similar resolution.

Wang *et al.*⁸ report a ring-shaped channel dimer that is substantially larger than our structure. The formation of dimers and the generally different appearance of the particles on the micrographs might reflect differences in the preparation protocol, in which Chaps was used to solubilize the channel and lipid added to stabilize the channel complex. The final structure was determined at a lower resolution and does not show any of the details we report here.

Materials and Methods

DHPR purification

DHPR was purified from rabbit skeletal muscle based on published protocols, yielding preparations with intact

dihydropyridine binding and functional activity after reconstitution in lipid bilayers.^{9,10} All procedures were carried out on ice or at 4 °C. Briefly, New Zealand White rabbit hind limb and back skeletal muscle was removed, homogenized, microsomes prepared by differential centrifugation and frozen in liquid nitrogen. The density of DHPR in the microsomes (9.4 pmol/mg) was determined by radioligand binding using (+)-[³H]PN200-110 (New England Nuclear; 79.7 Ci/mmol) as a specific ligand.¹⁰ A total of 448 mg of microsomal protein (6 mg/ml of membrane protein as determined by Lowry protein assay⁴⁵) were solubilized in 224 ml of 1% (w/v) digitonin (Biosynth, Switzerland; water-soluble), 0.5 M NaCl, 50 mM Tris-HCl (pH 7.4), 1 mM iodoacetamide, 0.1 mM benzamidine, 0.1 mM PMSF) for 40 minutes at 4 °C. Insoluble material was removed by centrifugation (50,000g for ten minutes). Solubilized channels were reversibly labeled with (+)-[³H]PN200-110 and loaded onto a wheat-germ agglutinin (WGA) Sepharose lectin-affinity column (15 ml gel). Chromatography was carried out using a peristaltic pump and low-pressure columns (BioRad Inc.) in standard buffer (50 mM Tris-HCl (pH 7.4), 25 μM CaCl₂, 1 mM iodoacetamide, 0.1 mM benzamidine, 0.1 mM PMSF, 0.1% (w/v) digitonin) with 150 mM NaCl. Unbound protein was removed with standard buffer and eluted in standard buffer containing 50 mM NaCl and 0.5 M *N*-acetyl-glucosamine. Aliquots (50 μl) were examined for radioactivity and protein concentration (Bradford protein assay; BioRad Inc.). DHPR-containing fractions were pooled and loaded onto a 20 ml DEAE Sepharose column pre-equilibrated in standard buffer and eluted with a 0.1 M–0.5 M salt gradient in standard buffer. Active fractions were pooled and layered onto three 40 ml 5%–20% (w/w) continuous sucrose gradients (in standard buffer) followed by velocity density centrifugation at 50,000 rpm for 90 minutes in a Beckman VTi50 vertical gradient rotor. Gradients were fractionated bottom up. Pooled active fractions were concentrated in a final step on a WGA column and frozen in liquid nitrogen as 50 μl aliquots. Final concentrations of purified fractions were up to 350 μg/ml of protein as determined with the Bradford assay (BioRad Inc.). The overall purification factor starting from solubilized membranes was 400×. Subunit composition was confirmed by SDS-PAGE analysis (using 7% or 10% (w/v) polyacrylamide separating gels; Mini Protean II, BioRad) followed by staining with Coomassie brilliant blue or silver (Figure 1A). Samples were denatured for three minutes at 95 °C in electrophoresis sample buffer containing 4% (w/v) SDS and 10 mM dithiothreitol (reducing conditions) or 10 mM *N*-ethyl-maleimide (non-reducing conditions). Gel bands were imaged on a Chemi Doc transilluminator (BioRad, Inc.) and quantitized using BioRad Quantity One v4.1.1 software. The identities of the α₁, α₂ and β subunits were confirmed by Western blot using monoclonal antibodies directed against α₁ (Sigma-Aldrich cat. no. D-218), α₂ (Affinity Bioreagents cat. no. MA3-921 anti-DHPR-α₂, mouse IgG_{2a}; Morton & Froehner, clone 20A) and β (Upstate Biotech, NY, cat. no. 05-264, clone V02-1812, mouse IgG₁). Labeled bands were visualized with alkaline-phosphatase coupled secondary anti-mouse IgG using the BCIP/NBT system (Pierce). Sedimentation velocity analysis was performed on a Beckman XLA analytical ultracentrifuge using a TLA 100.1 rotor at 50,000 rpm and resulting data were evaluated using the program SEDFIT⁴⁶ with the continuous *c*(*s*) distribution model. A sedimentation value of 8.8 S was determined as a prominent peak, indicating little

aggregation and predominantly monodisperse particles. There is a small secondary peak, indicating possible dissociation of some of the channel complexes.

Electron microscopy

Negative stain electron microscopy

Samples (4 μl; approximately 100 μg/ml as determined with Bradford/BioRad Protein Assay) were applied for one minute onto negatively glow-discharged carbon-coated grids, washed by flotation on three drops of buffer without detergent (50 mM Tris-HCl (pH 7.4), 150 mM NaCl, 25 μM CaCl₂) for ten seconds each and stained by flotation on three drops of 1% (w/v) uranyl acetate solution for ten seconds each, immediately blotting off excess stain with filter paper. Images were taken on a Philips CM12 electron microscope with a LaB₆ cathode operating at 120 kV, at a magnification of 60,000× under low-dose conditions (<10 e⁻/Å²) and defocus between 1.5 μm and 2.5 μm.

Electron cryo-microscopy

Samples (5 μl; approximately 350 μg/ml as determined with Bradford/BioRad Protein Assay) were applied to negatively glow-discharged holey carbon film (Quantifoil®). After blotting off excess liquid with filter paper (Whatman) for five to ten seconds at ~80% relative humidity, grids were plunged into liquid ethane using a cryo plunger. Vitrified samples were stored in liquid nitrogen and transferred to a Gatan cryo holder at liquid nitrogen temperature. Images were observed on an FEI Tecnai F20 electron cryo-microscope equipped with a field emission gun operating at 200 kV. Areas of interest were selected at low magnification and extremely low-dose by use of a Gatan 2000 × 2000 CCD camera. A total of 180 micrographs were taken under low-dose conditions (<10 e⁻/Å²) at a magnification of 62,000× and defocus between 3.0 μm and 4.5 μm.

Micrographs of both negatively stained and cryo samples were recorded on Kodak SO163 image film and developed for 12 minutes in full-strength D19.

Image processing

Micrographs were digitized with a Zeiss SCAI scanner at a step size of 7 μm. The scanned data from cryo samples were compressed threefold, resulting in a final pixel size of 3.39 Å/pixel at the specimen level. Data of samples in negative stain were compressed fourfold, corresponding to 4.67 Å/pixel at the specimen level. Astigmatism and defocus values were determined for each image using the program CTFIND3.⁴⁷ A total of 7550 individual particles were collected for the negative stain dataset and 15,229 particles for the cryo dataset using the MRC program XIMDISP.⁵³ Image processing was performed for both datasets independently using the IMAGIC software suite.¹² Five rounds of classification with subsequent multi-reference alignment yielded class average images with low intra-class variance. Characteristic side views were used to build an initial 3D model. More class averages were added stepwise and refined. The cycle back-projection–multi-reference alignment–classification–3D-reconstruction was iterated 18 times. The program FREALIGN,¹³ running parallelized on a PC cluster was used to correct each image for defocus and for further refinement of particle orientations. In all, 8% of all particles were discarded

based on a phase residual criterion. The final reconstruction of the cryo dataset included 14,056 particles and was sharpened with a negative temperature factor of 500. The resolution was determined according to the commonly used FSC of 0.5 obtained from a split dataset. The absolute handedness of the DHPR was not determined.

Immunolabeling

Two 180 μ l aliquots of purified DHPR protein (~ 300 μ g/ml) were dialyzed for two hours against 50 mM Tris-HCl (pH 7.4), 150 mM NaCl, 25 μ M CaCl₂, 0.1% (w/v) digitonin, in Slide-a-Lyzer cartridges (Pierce). Monoclonal antibody (20 μ l; anti- α_2 : affinity Bioreagents cat. no. MA3-921 anti-DHPR- α_2 , mouse IgG_{2a}; Morton & Froehner, clone 20A; anti- β : upstate Biotech, NY, cat. no. 05-264, clone V02-1812, mouse IgG₁) corresponding to a molar ratio of 1:10 (DHPR/IgG) were added to the dialysis chamber and incubated for three hours at 4 °C. Incubation mixtures (200 μ l) were injected onto a pre-equilibrated Superdex 200 PC 3.2/30 gel-filtration column connected to an Aekta FPLC system (Amersham Pharmacia Biotech). For comparison and calibration of molecular masses, an equivalent amount of purified DHPR and a gel-filtration standard (BioRad) were both run under identical conditions and the data were fit to an exponential function. Fractions containing active DHPR were identified by radioligand binding using (+)-[³H]PN200-110 and a filter-precipitation assay as described.¹⁰ Antibody-containing fractions were identified *via* dot-blot on a nitrocellulose membrane (3 μ l sample/fraction) with a secondary HRP-conjugated anti-mouse IgG antibody (New England Biolabs) and visualized by color reaction with BZIP/NBT (Pierce). Two intensity peaks (at fractions corresponding to a molecular mass of ~ 800 kDa and free antibody at ~ 150 kDa) were clearly resolved. Fractions (4 μ l) from samples with an apparent molecular mass of ~ 800 kDa were applied to negatively glow-discharged EM grids, washed and stained with 1% uranyl acetate as described above. Samples were examined with a Philips CM12 electron microscope operating at 120 kV at 60,000 \times magnification and micrographs were taken under low-dose conditions (~ 10 e⁻/Å²) and a defocus of 1.8 μ m. Micrographs were digitized on a Zeiss SCAI scanner as described above. Single images of individual antibody-DHPR complexes were picked according to visual recognition of the Y-shaped antibody using the MRC program XIMDISP.⁵³ Six characteristic views were selected from approximately 200 images of each anti- α_2 and anti- β channel conjugates.

Acknowledgements

We thank T. Walz & Y. Cheng for use of the Harvard EM facility, as well as C. Miller for comments on the manuscript, and M. Rigney for assistance with the membrane protein preparation. We are grateful to T. Wagenknecht and M. Samsó for providing the 3D reconstruction of RyR1, and K. Beam, R. Coronado and C. Franzini-Armstrong for valuable discussion. This work was supported by NIH grant 1 P01 GM-62580 (to N.G.) and the

Austrian Science Foundation (FWF P12689-MOB to H.G., P-14820 to J.S.).

References

- Reuter, H. (1983). Calcium channel modulation by neurotransmitters, enzymes and drugs. *Nature*, **301**, 569–574.
- De Jongh, K. S., Warner, C. & Catterall, W. A. (1990). Subunits of purified calcium channels. Alpha 2 and delta are encoded by the same gene. *J. Biol. Chem.* **265**, 14738–14741.
- Jay, S. D., Sharp, A. H., Kahl, S. D., Vedvick, T. S., Harpold, M. M. & Campbell, K. P. (1991). Structural characterization of the dihydropyridine-sensitive calcium channel alpha 2-subunit and the associated delta peptides. *J. Biol. Chem.* **266**, 3287–3293.
- Lapie, P., Lory, P. & Fontaine, B. (1997). Hypokalemic periodic paralysis: an autosomal dominant muscle disorder caused by mutations in a voltage-gated calcium channel. *Neuromuscul. Disord.* **7**, 234–240.
- Grabner, M., Dirksen, R. T., Suda, N. & Beam, K. G. (1999). The II–III loop of the skeletal muscle dihydropyridine receptor is responsible for the Bi-directional coupling with the ryanodine receptor. *J. Biol. Chem.* **274**, 21913–21919.
- Murata, K., Odahara, N., Kuniyasu, A., Sato, Y., Nakayama, H. & Nagayama, K. (2001). Asymmetric arrangement of auxiliary subunits of skeletal muscle voltage-gated l-type Ca(2+) channel. *Biochem. Biophys. Res. Commun.* **282**, 284–291.
- Serysheva, I. I., Ludtke, S. J., Baker, M. R., Chiu, W. & Hamilton, S. L. (2002). Structure of the voltage-gated L-type Ca²⁺ channel by electron cryomicroscopy. *Proc. Natl Acad. Sci. USA*, **99**, 10370–10375.
- Wang, M. C., Velarde, G., Ford, R. C., Berrow, N. S., Dolphin, A. C. & Kitmitto, A. (2002). 3D structure of the skeletal muscle dihydropyridine receptor. *J. Mol. Biol.* **323**, 85–98.
- Florio, V., Striessnig, J. & Catterall, W. A. (1992). Purification and reconstitution of skeletal muscle calcium channels. *Methods Enzymol.* **207**, 529–546.
- Striessnig, J. & Glossman, H. (1991). Purification of L-type calcium channel drug receptors. *Methods Neurosci.* **4**, 210–229.
- De Jongh, K. S., Warner, C., Colvin, A. A. & Catterall, W. A. (1991). Characterization of the two size forms of the alpha 1 subunit of skeletal muscle L-type calcium channels. *Proc. Natl Acad. Sci. USA*, **88**, 10778–10782.
- van Heel, M., Harauz, G., Orlova, E. V., Schmidt, R. & Schatz, M. (1996). A new generation of the IMAGIC image processing system. *J. Struct. Biol.* **116**, 17–24.
- Grigorieff, N. (1998). Three-dimensional structure of bovine NADH:ubiquinone oxidoreductase (complex I) at 22 Å in ice. *J. Mol. Biol.* **277**, 1033–1046.
- Quillin, M. L. & Matthews, B. W. (2000). Accurate calculation of the density of proteins. *Acta Crystallog. sect. D*, **56**, 791–794.
- Gurnett, C. A., De Waard, M. & Campbell, K. P. (1996). Dual function of the voltage-dependent Ca²⁺ channel alpha 2 delta subunit in current stimulation and subunit interaction. *Neuron*, **16**, 431–440.
- Catterall, W. A. (2000). Structure and regulation of voltage-gated Ca²⁺ channels. *Annu. Rev. Cell Dev. Biol.* **16**, 521–555.
- Huber, I., Wappl, E., Herzog, A., Mitterdorfer, J.,

- Glossmann, H., Langer, T. & Striessnig, J. (2000). Conserved Ca^{2+} -antagonist-binding properties and putative folding structure of a recombinant high-affinity dihydropyridine-binding domain. *Biochem. J.* **347**, 829–836.
18. Gurnett, C. A., Felix, R. & Campbell, K. P. (1997). Extracellular interaction of the voltage-dependent Ca^{2+} channel $\alpha_2\delta$ and α_1 subunits. *J. Biol. Chem.* **272**, 18508–18512.
19. Jay, S. D., Ellis, S. B., McCue, A. F., Williams, M. E., Védvick, T. S., Harpold, M. M. & Campbell, K. P. (1990). Primary structure of the gamma subunit of the DHP-sensitive calcium channel from skeletal muscle. *Science*, **248**, 490–492.
20. Arikath, J., Chen, C. C., Ahern, C., Allamand, V., Flanagan, J. D., Coronado, R. *et al.* (2003). Gamma 1 subunit interactions within the skeletal muscle L-type voltage-gated calcium channels. *J. Biol. Chem.* **278**, 1212–1219.
21. Freise, D., Held, B., Wissenbach, U., Pfeifer, A., Trost, C., Himmerkus, N. *et al.* (2000). Absence of the gamma subunit of the skeletal muscle dihydropyridine receptor increases L-type Ca^{2+} currents and alters channel inactivation properties. *J. Biol. Chem.* **275**, 14476–14481.
22. De Waard, M., Scott, V. E., Pragnell, M. & Campbell, K. P. (1996). Identification of critical amino acids involved in α_1 - β interaction in voltage-dependent Ca^{2+} channels. *FEBS Letters*, **380**, 272–276.
23. Pragnell, M., De Waard, M., Mori, Y., Tanabe, T., Snutch, T. P. & Campbell, K. P. (1994). Calcium channel β -subunit binds to a conserved motif in the I–II cytoplasmic linker of the α_1 subunit. *Nature*, **368**, 67–70.
24. Witcher, D. R., De Waard, M., Liu, H., Pragnell, M. & Campbell, K. P. (1995). Association of native Ca^{2+} channel β subunits with the α_1 subunit interaction domain. *J. Biol. Chem.* **270**, 18088–18093.
25. Sokolova, O., Kolmakova-Partensky, L. & Grigorieff, N. (2001). Three-dimensional structure of a voltage-gated potassium channel at 2.5 nm resolution. *Structure (Camb.)*, **9**, 215–220.
26. Smith, E. L. & Pickels, E. G. (1940). Micelle formation in aqueous solutions of digitonin. *Proc. Natl Acad. Sci. USA*, **26**, 272–277.
27. Avelldano, M. I. (1995). Phospholipid solubilization during detergent extraction of rhodopsin from photoreceptor disk membranes. *Arch. Biochem. Biophys.* **324**, 331–343.
28. Horne, W. A., Weiland, G. A. & Oswald, R. E. (1986). Solubilization and hydrodynamic characterization of the dihydropyridine receptor from rat ventricular muscle. *J. Biol. Chem.* **261**, 3588–3594.
29. Block, B. A., Imagawa, T., Campbell, K. P. & Franzini-Armstrong, C. (1988). Structural evidence for direct interaction between the molecular components of the transverse tubule/sarcoplasmic reticulum junction in skeletal muscle. *J. Cell Biol.* **107**, 2587–2600.
30. Protasi, F., Franzini-Armstrong, C. & Flucher, B. E. (1997). Coordinated incorporation of skeletal muscle dihydropyridine receptors and ryanodine receptors in peripheral couplings of BC3H1 cells. *J. Cell Biol.* **137**, 859–870.
31. Samsó, M., Trujillo, R., Gurrola, G. B., Valdivia, H. H. & Wagenknecht, T. (1999). Three-dimensional location of the imperatoxin A binding site on the ryanodine receptor. *J. Cell Biol.* **146**, 493–499.
32. Jiang, Y., Lee, A., Chen, J., Ruta, V., Cadene, M., Chait, B. T. & MacKinnon, R. (2003). X-ray structure of a voltage-dependent K^{+} channel. *Nature*, **423**, 33–41.
33. Bichet, D., Cornet, V., Geib, S., Carlier, E., Volsen, S., Hoshi, T. *et al.* (2000). The I–II loop of the Ca^{2+} channel α_1 subunit contains an endoplasmic reticulum retention signal antagonized by the β subunit. *Neuron*, **25**, 177–190.
34. Beurg, M., Ahern, C. A., Vallejo, P., Conklin, M. W., Powers, P. A., Gregg, R. G. & Coronado, R. (1999). Involvement of the carboxy-terminus region of the dihydropyridine receptor β_1 subunit in excitation–contraction coupling of skeletal muscle. *Biophys. J.* **77**, 2953–2967.
35. Cheng, W. & Coronado, R. (2003). Biophysical soc. 47th annual meeting, Poster 526: direct binding of skeletal dihydropyridine receptor β subunit to ryanodine receptor type I. *Biophys. J.* **84**, 109a.
36. Samsó, M. & Wagenknecht, T. (2002). Apocalmodulin and Ca^{2+} -calmodulin bind to neighboring locations on the ryanodine receptor. *J. Biol. Chem.* **277**, 1349–1353.
37. Haarmann, C. C., Green, D., Casarotto, M. G., Laver, D. R. & Dulhunty, A. F. (2003). The random coil C fragment of the DHPR II III loop can activate or inhibit native skeletal RyRs. *Biochem. J.* **372**, 305–316.
38. Proenza, C., O'Brien, J., Nakai, J., Mukherjee, S., Allen, P. D. & Beam, K. G. (2002). Identification of a region of RyR1 that participates in allosteric coupling with the α_1 (S) ($\text{Ca(V)}1.1$) II–III loop. *J. Biol. Chem.* **277**, 6530–6535.
39. Zhang, J., Liu, Z., Masumiya, H., Wang, R., Jiang, D., Li, F. R. *et al.* (2003). Three-dimensional localization of divergent region 3 of the ryanodine receptor to the clamp-shaped structures adjacent to the FKBP binding sites. *J. Biol. Chem.*
40. Papadopoulos, S., Leuranguer, V. & Beam, K. G. (2003). Biophysical soc. 47th annual meeting, poster 2802: fluorescence resonance energy transfer (FRET) between β_1 and α_1 S subunit of the skeletal muscle DHPR receptor. *Biophys. J.* **84**, 573a.
41. Lipkind, G. M. & Fozzard, H. A. (2001). Modeling of the outer vestibule and selectivity filter of the L-type Ca^{2+} channel. *Biochemistry*, **40**, 6786–6794.
42. Wagenknecht, T., Radermacher, M., Grassucci, R., Berkowitz, J., Xin, H. B. & Fleischer, S. (1997). Locations of calmodulin and FK506-binding protein on the three-dimensional architecture of the skeletal muscle ryanodine receptor. *J. Biol. Chem.* **272**, 32463–32471.
43. Wagenknecht, T., Hsieh, C. E., Rath, B. K., Fleischer, S. & Marko, M. (2002). Electron tomography of frozen-hydrated isolated triad junctions. *Biophys. J.* **83**, 2491–2501.
44. Yin, C. C. & Lai, F. A. (2000). Intrinsic lattice formation by the ryanodine receptor calcium-release channel. *Nature Cell Biol.* **2**, 669–671.
45. Lowry, O. H., Rosebrough, N. J., Farr, A. L. & Randall, R. J. (1951). Protein measurement with the folin-phenol reagents. *J. Biol. Chem.* **193**, 265–275.
46. Schuck, P. (2000). Size-distribution analysis of macromolecules by sedimentation velocity ultracentrifugation and lamm equation modeling. *Biophys. J.* **78**, 1606–1619.
47. Mindell, J. A. & Grigorieff, N. (2003). Accurate determination of local defocus and specimen tilt in electron microscopy. *J. Struct. Biol.* **142**, 334–347.
48. Huang, C. C., Couch, G. S., Pettersen, E. F. & Ferrin, T. E. (1996). Chimera: an extensible molecular modeling

- application constructed using standard components. *Pac. Symp. Biocomput.* **1**, 724.
49. Takekura, H., Nishi, M., Noda, T., Takeshima, H. & Franzini-Armstrong, C. (1995). Abnormal junctions between surface membrane and sarcoplasmic reticulum in skeletal muscle with a mutation targeted to the ryanodine receptor. *Proc. Natl Acad. Sci. USA*, **92**, 3381–3385.
 50. Baker, M. L., Serysheva, I. I., Sencer, S., Wu, Y., Ludtke, S. J., Jiang, W. *et al.* (2002). The skeletal muscle Ca²⁺ release channel has an oxidoreductase-like domain. *Proc. Natl Acad. Sci. USA*, **99**, 12155–12160.
 51. Liu, Z., Zhang, J., Sharma, M. R., Li, P., Chen, S. R. & Wagenknecht, T. (2001). Three-dimensional reconstruction and localization of its amino terminus. *Proc. Natl Acad. Sci. USA*, **98**, 6104–6109.
 52. Liu, Z., Zhang, J., Li, P., Chen, S. R. & Wagenknecht, T. (2002). Three-dimensional reconstruction of the recombinant type 2 ryanodine receptor and localization of its divergent region 1. *J. Biol. Chem.* **277**, 46712–46719.
 53. Smith, J. M. (1999). XIMDISP – a visualization tool to aid structure determination from electron microscope images. *J. Struct. Biol.* **125**, 223–228.

Edited by Sir A. Klug

(Received 12 May 2003; received in revised form 23 June 2003; accepted 11 July 2003)